

Electromagnetic response and effective gauge theory of graphene in a magnetic field

K. Shizuya

*Yukawa Institute for Theoretical Physics
Kyoto University, Kyoto 606-8502, Japan*

The electromagnetic response of graphene in a magnetic field is studied, with particular emphasis on the quantum features of its ground state (vacuum). The graphene vacuum, unlike in conventional quantum Hall systems, is a dielectric medium and carries an appreciable amount of electric and magnetic susceptibilities. The dielectric effect grows rapidly with increasing filling factor ν in such a way that reflects the ‘relativistic’ Landau-level characteristics of graphene as well as its valley and spin degeneracy. A close look into the dielectric function also reveals that the Coulomb interaction is efficiently screened on the scale of the magnetic length, leading to a prominent reduction of the exciton spectra in graphene. In addition, an effective gauge theory of graphene is constructed out of the response. It is pointed out thereby that the electric susceptibility is generally expressed as a ratio of the Hall conductance to the Landau gap.

PACS numbers: 73.43.-f, 71.10.Pm, 77.22.Ch

I. INTRODUCTION

There has recently been increasing interest, both experimentally^{1,2,3} and theoretically^{4,5,6,7,8,9,10}, in a ‘relativistic’ condensed-matter system, graphene which is a monolayer of graphite. Graphene is a gapless planar semiconductor, in which low-energy electronic transport is essentially governed by massless Dirac fermions with effective speed of light $v_F \approx 10^6$ m/s $\approx c/300$, and thus provides a special opportunity to study relativistic quantum dynamics in condensed-matter systems. Experiments have revealed a number of exotic transport properties of graphene, such as an unusual sequence^{1,2} of magneto-oscillations and of the quantum Hall (QH) effect, that are characteristic of Dirac fermions.

It has long been known that Dirac electrons in 2+1 dimensions lead to peculiar quantum phenomena of fractional fermion number¹¹: Fractional charge and current of abnormal parity, as summarized by the Chern-Simons (CS) term, are induced in the vacuum in response to an applied field. The induced CS term, or a parity anomaly, is associated with a spectral asymmetry and an index of the Dirac Hamiltonian, and is also tied to the chiral anomaly in 1+1 dimensions¹². The one-half degeneracy of the lowest Landau level observed^{1,2} in the graphene QH effect is a manifestation of fermion number fractionalization, although complete cancellation of the net vacuum charge and current takes place in graphene (which involves a parity pair of fermions).

The purpose of this paper is to explore possible signatures of relativistic quantum field theory in the low-energy physics of graphene. We study the electromagnetic response of graphene in a magnetic field at integer filling factor ν , with particular emphasis on the quantum features of the ground state with $\nu = 0$, the vacuum state. For graphene, unlike standard QH systems, the vacuum state is a dielectric medium and carries an appreciable amount of both electric and magnetic suscep-

tibilities (α_e, α_m) over the entire range of wavelengths; this reflects the presence of the ‘Dirac sea’. The dielectric effect grows rapidly with increasing filling factor ν in such a way that reflects the ‘relativistic’ Landau-level characteristics of graphene as well as its valley and spin degeneracy. A close look into the dielectric function reveals that the Coulomb interaction is efficiently screened on the scale of the magnetic length, leading to a prominent reduction of the exciton spectra in graphene.

In addition, we construct, out of the response and via functional bosonization, a low-energy effective gauge theory of graphene in a magnetic field. It is pointed out thereby that the electric susceptibility α_e is generally expressed as a ratio of the Hall conductance to the Landau gap.

In Sec. II we study the electromagnetic response of graphene in a magnetic field, with emphasis on projection to Landau levels and regularization. In Sec. III we construct an effective theory of graphene. In Sec. IV we discuss the effect of polarization by treating the Coulomb interaction in the random-phase approximation (RPA). Section V is devoted to a summary and discussion.

II. ELECTROMAGNETIC RESPONSE

Graphene has a honeycomb lattice which consists of two triangle sublattices of carbon atoms with one electron per site. The electrons are described by a two-component spinor $(U, V)^t$ with fields U and V residing on each sublattice. In the tight-binding approximation with nearest neighbor interactions the spectrum of electrons becomes linear at the two inequivalent Fermi points (K and K') on the corners of the Brillouin zone. In the continuum limit the system is described by a low-energy effective

Hamiltonian of the form¹³

$$H = \int d^2\mathbf{x} [\psi^\dagger \mathcal{H}_+ \psi + \chi^\dagger \mathcal{H}_- \chi],$$

$$\mathcal{H}_\pm = v_F (\sigma_1 \Pi_1 + \sigma_2 \Pi_2 \pm m \sigma_3) - e A_0, \quad (2.1)$$

with coupling to external electromagnetic potentials $A_\mu = (A_i, A_0)$ introduced through $\Pi_i = -i\partial_i + eA_i$ [$i = (1, 2)$ or (x, y)]; $v_F \sim 10^6$ m/s is the Fermi velocity. Here ψ and χ stand for the electron fields near the K and K' points (at wave vectors $\mp \mathbf{q}$) and have the structure $\psi_\alpha = (\psi_1, \psi_2)^t \propto (U_{\mathbf{k}-\mathbf{q}}, V_{\mathbf{k}-\mathbf{q}})^t$ and $\chi_\alpha = (\chi_1, \chi_2)^t \propto (-V_{\mathbf{k}+\mathbf{q}}, U_{\mathbf{k}+\mathbf{q}})^t$, where $U_{\mathbf{k}} = U_{\mathbf{k}}(t)$, e.g., denotes the Fourier transform of $U(\mathbf{x}, t)$ for short.

For generality we have introduced a tiny ‘mass’ gap m , which works to lift the degeneracy of the lowest ($n = 0$) Landau level alone. The possibility of such a mass gap has been discussed^{7,8,9,10} in connection with the observed lifting³ of the degeneracy of the $n = 0, 1$ levels in high magnetic fields. Nonzero mass $m \neq 0$ spoils the pseudospin (or sublattice) $SU(2)$ symmetry of H , which rotates (ψ, χ) . Actually, we keep $m \neq 0$ to reveal the particle/hole character of the $n=0$ levels, as remarked below, and set $m \rightarrow 0$ eventually.

For clarity, we suppress the electron spin, which is treated as a global $SU(2)$ symmetry of H by doubling the fields, ψ^a and χ^a with $a = (\uparrow, \downarrow)$. The $SU(2)$ -breaking Zeeman coupling is considerably weak, compared with the Coulomb interaction, for graphene and is ignored in the following.

The Coulomb interaction is written as

$$H^{\text{Coul}} = \frac{1}{2} \sum_{\mathbf{p}} v_{\mathbf{p}} \rho_{-\mathbf{p}} \rho_{\mathbf{p}}, \quad (2.2)$$

where $\rho_{\mathbf{p}}$ is the Fourier transform of the electron number density $\rho = \psi^\dagger \psi + \chi^\dagger \chi$; $v_{\mathbf{p}} = 2\pi\alpha/(\epsilon_b |\mathbf{p}|)$ is the Fourier transform of the Coulomb potential $v(\mathbf{x}) = \alpha/(\epsilon_b |\mathbf{x}|)$ with the fine-structure constant $\alpha = e^2/(4\pi\epsilon_0) \approx 1/137$ and the substrate dielectric constant ϵ_b . In this paper we shall focus on the long-wavelength properties of graphene and consider $H + H^{\text{Coul}}$ as our basic Hamiltonian; other short-distance corrections⁸, including the oscillating piece $\propto e^{\pm 2i\mathbf{q}\cdot\mathbf{x}}$ of the Coulomb interaction, will thus be ignored.

Let us place graphene in a strong magnetic field and first study how the electrons in graphene respond to weak external potentials $A_\mu(x)$. To this end we set $A_i(x) \rightarrow A_i^B(\mathbf{x}) + A_i(\mathbf{x}, t)$ in the Hamiltonian (2.1), where the vector potential $\mathbf{A}^B = B(-y, 0)$ supplies a uniform magnetic field $B_z = B > 0$ normal to the graphene plane. We turn off H^{Coul} for the moment.

When $A_\mu = 0$, the eigenmodes of H are Landau levels of ψ and χ of energy

$$\epsilon_n = s_n \omega_c \sqrt{|n| + \frac{1}{2} m^2 \ell^2}, \quad (2.3)$$

labeled by integers $n = 0, \pm 1, \pm 2, \dots$, and p_x (or $y_0 \equiv \ell^2 p_x$ with the magnetic length $\ell \equiv 1/\sqrt{eB}$); $\omega_c = \sqrt{2} v_F / \ell$

is the basic cyclotron frequency. Here $s_n \equiv \text{sign}\{n\} (= \pm 1)$ specifies the sign of the energy ϵ_n .

For each $n \neq 0$, ψ and χ have the same spectra and the positive- and negative-energy (i.e., $n > 0$ and $n < 0$) levels are symmetric in structure. [This is a consequence of the conjugation symmetry $\mathcal{H}_+ = -\sigma_3(\mathcal{H}_-)\sigma_3$ with $A_0 = 0$.] The $n = 0$ spectra depend on the sign of m . Let us take $m > 0$. Then the $n = 0$ level of ψ has negative energy $\epsilon_{0-} = -v_F m$ while that of χ has positive energy $\epsilon_{0+} = v_F m$. These $n = 0_\mp$ levels represent holes and electrons via quantization; and this hole/particle characterization persists even in the limit $m \rightarrow 0$ where the $n = 0_\mp$ levels become degenerate. These $n = 0_\pm$ eigenmodes have components only on each separate sublattice; see Appendix A for details of the wave functions. With the electron spin taken into account, each Landau level is thus four-fold degenerate, except for the $n = 0_\pm$ levels which are doubly-degenerate.

To make this Landau-level structure explicit, it is useful to pass to the $|n, y_0\rangle$ basis, with the expansion $\psi(\mathbf{x}, t) = \sum_{n, y_0} \langle \mathbf{x} | n, y_0 \rangle \psi_n(y_0, t)$. (From now on, we shall only display the ψ sector since the χ sector is obtained by reversing the sign of m .) The translation is simple^{14,15}: In the $|n, y_0\rangle$ representation the coordinate $\mathbf{x} = (x_1, x_2)$ of $A_\mu(\mathbf{x}, t)$ is split into the center coordinate $\mathbf{r} = (r_1, r_2) = (i\ell^2 \partial / \partial y_0, y_0)$ with uncertainty $[r_1, r_2] = i\ell^2$ and the relative coordinate $\mathbf{X} = (X_1, X_2)$ with $[X_1, X_2] = -i\ell^2$ which are matrices in the Landau-level index. The Hamiltonian H thereby is rewritten as

$$H = \int dy_0 \sum_{n, n' = -\infty}^{\infty} \psi_n^\dagger(y_0, t) \{ \epsilon_n \delta_{nn'} + e V_{nn'} \} \psi_{n'}(y_0, t),$$

$$V_{nn'} = v_F \mathcal{A}_{nn'} + v_F \mathcal{A}_{nn'}^\dagger - (\mathcal{A}_0)_{nn'}. \quad (2.4)$$

Here the electromagnetic coupling $V_{nn'}$ is a matrix in the level index and a function of $\mathbf{r} = (i\ell^2 \partial / \partial y_0, y_0)$: The field

$$(\mathcal{A}_0)_{nn'}(\mathbf{r}, t) = \sum_{\mathbf{p}} e^{i\mathbf{p}\cdot\mathbf{r}} g_{nn'}(\mathbf{p}) e^{-\frac{1}{4} \ell^2 \mathbf{p}^2} (\mathcal{A}_0)_{\mathbf{p}} \quad (2.5)$$

is expressed in terms of the Fourier transform $(\mathcal{A}_0)_{\mathbf{p}}(t)$ of $A_0(\mathbf{x}, t)$ and the coefficient matrix

$$g_{nn'}(\mathbf{p}) = \frac{1}{2} \left[c_n^+ c_{n'}^+ f_{|n|-1, |n'|-1}(\mathbf{p}) + s_n s_{n'} c_n^- c_{n'}^- f_{|n|, |n'|}(\mathbf{p}) \right] \quad (2.6)$$

with $c_n^\pm = \sqrt{1 \pm v_F m / \epsilon_n}$, where

$$f_{kn}(\mathbf{p}) = \sqrt{\frac{n!}{k!}} \left(\frac{i\ell p}{\sqrt{2}} \right)^{k-n} L_n^{(k-n)} \left(\frac{1}{2} \ell^2 \mathbf{p}^2 \right) \quad (2.7)$$

for $k \geq n$; $p = p_y + ip_x$; for $k \leq n$ one may set $k \leftrightarrow n$ and $p \rightarrow p_y - ip_x$. Similarly, $\mathcal{A}_{nn'}$ is defined by Eq. (2.5) with $(\mathcal{A}_0)_{\mathbf{p}} \rightarrow (A_x + iA_y)_{\mathbf{p}}$ and

$$g_{nn'}(\mathbf{p}) \rightarrow j_{nn'}(\mathbf{p}) = \frac{1}{2} c_n^+ c_{n'}^- f_{|n|-1, |n'|}(\mathbf{p}); \quad (2.8)$$

$\mathcal{A}_{nn'}^\dagger$ is defined with $(A_x - iA_y)_\mathbf{p}$ and $j_{nn'}^\dagger(\mathbf{p}) \equiv j_{n'n}(-\mathbf{p})$. It is clear from Eq. (2.4) that $(A_0)_\mathbf{p}$ is coupled to the charge density $\rho_{-\mathbf{p}}(t) = \int d^2\mathbf{x} e^{i\mathbf{p}\cdot\mathbf{x}} \psi^\dagger \psi$ rewritten as

$$\rho_{-\mathbf{p}} = e^{-\frac{1}{4}\ell^2\mathbf{p}^2} \sum_{n,n'} g_{nn'}(\mathbf{p}) \int dy_0 \psi_n^\dagger e^{i\mathbf{p}\cdot\mathbf{r}} \psi_{n'}; \quad (2.9)$$

analogously for the current $J(x) = \frac{1}{2} \psi^\dagger (\sigma_1 + i\sigma_2) \psi$ coupled to $A = A_x + iA_y$.

Even a weak potential $A_\mu(x)$ causes mixing of the Landau levels, and its effect is calculated by diagonalizing H with respect to the true levels $\{n\}$ by a suitable $U(\infty)$ transformation $\psi_n^G(y_0, t) = \sum_m G_{nm}(\mathbf{r}, t) \psi_m(y_0, t)$. This yields $H = \int dy_0 \sum_n (\psi_n^G)^\dagger \mathcal{H}_{nn}^G \psi_n^G$ with $\mathcal{H}^G = G(\mathcal{H} - i\partial_t)G^{-1}$ diagonal in the level index. To $O(A_\mu^2)$, $\mathcal{H}_{nn}^G \equiv h_n = \epsilon_n + V_{nn} + V_n^{(2)}$ with

$$V_n^{(2)} = \frac{1}{2} \sum_k' \left\{ V_{nk} \frac{1}{\epsilon_n - \epsilon_k + i\partial_t} V_{kn} - (n \leftrightarrow k) \right\}, \quad (2.10)$$

where $i\partial_t$ acts on V_{kn} . This $O(V^2)$ term embodies the $\langle \rho\rho \rangle$ and $\langle JJ^\dagger \rangle$ correlation functions and constitutes the linear response of the system. Actually it only takes account of inter-Landau-level transitions due to the cyclotron modes; they govern the response of graphene at integer filling factors, on which we focus throughout this paper. For graphene at noninteger filling one encounters intra-level (collective) excitations,¹⁶ which are less sensitive to long-wavelength probes and are determined by diagonalizing the Coulomb Hamiltonian H^{Coul} projected to a given Landau level.

Let us now consider the long-wavelength part of the electromagnetic response, which, in view of gauge invariance, takes the form

$$h_n = \epsilon_n - eA_0 + \gamma_n \frac{1}{2} \epsilon^{\mu\nu\lambda} A_\mu \partial_\nu A_\lambda - \beta_n \frac{1}{2} e^2 (E_k)^2 + \eta_n \frac{1}{2} e^2 (A_{12})^2 + \dots, \quad (2.11)$$

where $E_k = -\partial_k A_0 - \partial_t A_x$ and $A_{12} = \partial_1 A_2 - \partial_2 A_1$; $\epsilon^{012} = 1$. Actual calculations are simplified if we take $A_\mu(\mathbf{x}, t)$ uniform in x_1 , i.e., $A_\mu(y, t)$. Then the CS term $\epsilon^{\mu\nu\lambda} A_\mu \partial_\nu A_\lambda \sim (A_y \dot{A}_x - A_x \dot{A}_y)$, the $E_i^2 \sim (\dot{A}_x)^2 + (\dot{A}_y)^2$ term and the $(A_{12})^2 \sim (\partial_y A_x)^2$ term are derived from the $O(\partial_t)$, $O(\partial_t^2)$ and $O(\mathbf{p}^2)$ parts of the $\langle JJ^\dagger \rangle$ response function, respectively. A direct calculation yields

$$\begin{aligned} \gamma_n &= e^2 \ell^2, \quad \beta_n = \ell^4 \frac{3\epsilon_n^2 - m^2 v_F^2}{2v_F^2 \epsilon_n}, \\ \eta_n &= \ell^4 \left(3 + \frac{m^2 v_F^2}{\epsilon_n^2} \right) \frac{(\epsilon_n^2 - m^2 v_F^2)}{4\epsilon_n}. \end{aligned} \quad (2.12)$$

Note that γ_n is independent of n while $\beta_{-n} = -\beta_n$ (with $\beta_{0\mp} = \mp |m| \ell^4 / v_F$) and $\eta_{-n} = -\eta_n$ (with $\eta_0 = 0$).

We are now ready to introduce the quantum vacuum as the Dirac sea with all negative-energy electron states occupied. Let us rename $a_n(y_0, t) = \psi_n^G(y_0, t)$ and

$d_n(y_0, t) = (\psi_n^G)^\dagger_{-n}(y_0, t)$ with $n > 0$ to denote electrons and holes over the vacuum. The Hamiltonian then reads

$$H = \int dy_0 \left[\sum_{n=1}^{\infty} h_n a_n^\dagger a_n - \sum_{n=0}^{\infty} h_{-n} d_n^\dagger d_n + \Delta \right], \quad (2.13)$$

$$\Delta = \delta_0 \sum_{n=0}^{\infty} h_{-n}, \quad (2.14)$$

where $\delta_0 \equiv \delta(y_0 = 0) = L_x / (2\pi \ell^2)$ stands for the degeneracy of each Landau level; $L_x = \int dx_1$.

Here Δ represents the quantum response of the vacuum. Apparently it is indeterminate because of the sums over an infinite number of Landau levels. Note, e.g., that $\gamma_n = e^2 \ell^2 > 0$ for all n . This would naively mean that the vacuum, the Dirac sea, carries an infinitely large Hall conductance, which is physically unacceptable. To obtain a sensible answer one has to define the sum carefully. For regularization let us truncate the spectrum to a finite number $(2N + 1)$ of Landau levels $\{n\}$ with $-\epsilon_N \leq \epsilon_n \leq \epsilon_N$, and let $N \rightarrow \infty$ at the end.¹⁸

It is instructive to see why and how this regularization works physically. Let us note that in $V_n^{(2)}$ of Eq. (2.10) the virtual $(n \rightarrow k \rightarrow n)$ transition and the related $(k \rightarrow n \rightarrow k)$ transition contribute equally but in opposite sign. For definiteness, we denote by F_n the $O(V^2)$ response, $\beta_n, \gamma_n, \eta_n, \dots$, collectively, and write it as the regularized sum $F_n = \sum_{k=-N}^N F_n^k$ over the contribution F_n^k from the $n \rightarrow k \rightarrow n$ subprocesses. Then, in the sum $\sum_n F_n$ cancellation takes place among a majority of terms, owing to the antisymmetry

$$F_n^k = -F_k^n, \quad (2.15)$$

which implies pair-wise cancellation between the $n \rightarrow k \rightarrow n$ and $k \rightarrow n \rightarrow k$ subprocesses. Fermi statistics is thus naturally taken care of in the regularized sum. Such a pair-wise cancellation of virtual processes is a basic property of Berry's phase^{17,19}; and it is also an exact property²⁰ of the density and current response functions (with also the Coulomb interaction included), as is clear from their spectral representations.

The vacuum response is now written as a regularized sum $\Delta = \delta_0 \sum_{n=0}^N h_{-n}$ or $F^{\text{vac}} \equiv \sum_{n>0}^N F_{-n}$. Note here that the regularized sum of F_n over all the levels vanishes, $\sum_{n=-N}^N F_n = \sum_n \sum_k F_n^k = 0$. This fact allows one to cast F^{vac} in another suggestive form

$$\sum_{n=-N}^{n_f} F_n = \frac{1}{2} \left(\sum_{n=-N}^{n_f} F_n - \sum_{n>n_f}^N F_n \right). \quad (2.16)$$

Here we have written the response in a slightly generalized form: The left-hand side is the response of a many-body state with Landau levels occupied up to $n = n_f$; the choice $n_f = 0_-$ thus yields F^{vac} . This formula expresses the quantum response in terms of an asymmetry in the spectrum of the occupied and empty levels, weighted with the response F_n per level.

Via regularization the calculation of the response is modified. A close look into the matrix elements in Eq. (2.8) shows that β_n and γ_n come only from virtual transitions to the adjacent levels ($n \rightarrow n \pm 1$) and the related ones across the Dirac sea ($n \rightarrow -\{n \pm 1\}$). As a result, the expressions for γ_n and β_n in Eq. (2.12) are valid for $|n| \leq N-1$ while the boundary contributions γ_{-N} and β_{-N} have to be calculated from the $-N \rightarrow \pm(N-1) \rightarrow -N$ processes. For $\gamma_{\mp N}$ the result is

$$\gamma_{\mp N} = -e^2 \ell^2 (N - \frac{1}{2} \pm \frac{1}{2} m/\epsilon_N), \quad (2.17)$$

which then makes Δ^γ finite,

$$\Delta^\gamma = \delta_0 \sum_{n=0}^N \gamma_{-n} = \frac{1}{2} e^2 \ell^2 \delta_0 = L_x \frac{e^2}{4\pi\hbar}. \quad (2.18)$$

This implies that the vacuum would have Hall conductance equal to half of a filled level, $\sigma_{\text{Hall}}^{\text{vac}} = \frac{1}{2} e^2/h$, and that the Hall effect would arise without real electrons or holes. This nonzero Δ^γ is attributed to a spectral asymmetry due to the $n = 0_-$ level if one uses Eq. (2.16) (since $\gamma_{-N} - \gamma_N \rightarrow 0$), as normally implied by an index theorem¹². The physical mechanism underlying the vacuum Hall effect was discussed earlier^{19,21}. Actually, the χ sector contributes to Δ^γ in opposite sign and the vacuum Hall effect does not take place for graphene.

In contrast, the vacuum effect survives for susceptibilities β_n and η_n that change sign with n . For β_n the boundary contribution again increases rapidly with N ,

$$\beta_{\mp N} \approx \sqrt{2} (\ell^3/v_F) \left[\pm (N - \frac{1}{2} + \frac{1}{3} \lambda)^{3/2} + \frac{1}{2} \sqrt{\lambda} \right], \quad (2.19)$$

where $\lambda = \frac{1}{2} m^2 \ell^2$, and makes the vacuum electric susceptibility $\alpha_e^{\text{vac}} = (\sum_{n=1}^N \beta_{-n} + \beta_{0_-}) \delta_0/L_x$ finite,

$$\alpha_e^{\text{vac}} = \frac{3e^2}{2\pi\omega_c} \left\{ G(\lambda) - \frac{1}{3} \sqrt{\lambda} \right\}, \quad (2.20)$$

with

$$\begin{aligned} G(\lambda) &= - \sum_{n=1}^{N-1} \left\{ \sqrt{n+\lambda} - \frac{\lambda/3}{\sqrt{n+\lambda}} \right\} \\ &\quad + \frac{2}{3} \left(N - \frac{1}{2} + \frac{1}{3} \lambda \right)^{3/2}, \\ &= -\zeta(-\frac{1}{2}) - \lambda \frac{1}{6} \zeta(\frac{1}{2}) + \dots, \\ &\approx 0.2079 + \lambda \cdot 0.2434 + \dots \end{aligned} \quad (2.21)$$

Here we have used

$$\begin{aligned} \sum_{n=1}^{N-1} \sqrt{n} - \frac{2}{3} (N - \frac{1}{2})^{3/2} &= \zeta(-\frac{1}{2}) \approx -0.2079, \\ \sum_{n=1}^{N-1} 1/\sqrt{n} - 2\sqrt{N - \frac{1}{2}} &= \zeta(\frac{1}{2}) \approx -1.4604. \end{aligned} \quad (2.22)$$

It is instructive to derive this α_e^{vac} by selectively summing up the virtual ($-n \rightarrow n \pm 1 \rightarrow -n$) processes from

the Dirac sea. This reproduces $G(0)$ as the sum

$$6G(0) = 1 + \sum_{k=1}^{N-1} (\sqrt{n+1} - \sqrt{n})^3. \quad (2.23)$$

Formula (2.16) also leads to the same result (2.20). Note that this formula admits a further generalization: Instead of the symmetric spectral cutoff one can equally well truncate the positive- and negative-energy spectra independently by choosing $-N \leq n \leq N'$ so that there are $(N+N'+1)$ Landau levels in total. Clearly β_{-N} and γ_{-N} are unchanged if one takes $N' \geq N$.

With this generalization in mind let us now examine the magnetic susceptibility of the vacuum, $\alpha_m^{\text{vac}} = (\sum_{n=1}^N \eta_{-n} + \eta_{0_-}) \delta_0/L_x$. A look into the matrix elements again reveals that the expression (2.12) for η_n is valid only for $|n| \leq N-2$. Also a direct calculation shows that the virtual transitions from the bottom of the Dirac sea to positive-energy states *combine*²² to vanish (for $N \rightarrow \infty$) once one takes $N' \geq N+2$, and the response is independent of the way one sends $(N, N') \rightarrow \infty$. We therefore set $N' \geq N+2$ to calculate the boundary term $\eta_{-N} + \eta_{-(N-1)}$ and obtain

$$\alpha_m^{\text{vac}} = \frac{3e^2 v_F^2}{4\pi\omega_c} G_m(\lambda), \quad (2.24)$$

with

$$\begin{aligned} G_m(\lambda) &= - \sum_{n=1}^N \frac{n}{n+\lambda} \left(\sqrt{n+\lambda} + \frac{\lambda/3}{\sqrt{n+\lambda}} \right) \\ &\quad + \frac{2}{3} \left(N + \frac{1}{2} - \frac{1}{3} \lambda \right)^{3/2}, \\ &= -\zeta(-\frac{1}{2}) + \frac{\lambda}{6} \zeta(\frac{1}{2}) + \dots, \\ &\approx 0.2079 - \lambda \cdot 0.2434 + \dots \end{aligned} \quad (2.25)$$

Let us next consider the A_0 response in h_n , which probes the charge of the system. The observable charge is a difference between the $B \neq 0$ and $B = 0$ cases. Such an induced charge is detected by a normal-ordered charge operator $:\psi_n^\dagger \psi_n: = \frac{1}{2} [\psi_n^\dagger, \psi_n]$ and a symmetric spectral cutoff, with the result¹²

$$\Delta Q^{\text{vac}} = \frac{e}{2} \frac{1}{2\pi\ell^2} = e^2 B/(4\pi) \quad (2.26)$$

per unit area. Alternatively, this induced charge is derived from Δ^γ in Eq. (2.18) if one notes that the variation of ΔQ under the change $B \rightarrow B + A_{12}$ is read from the CS coupling. It is thus clear that there is no induced vacuum charge in graphene.

Similarly, one can calculate the observable vacuum energy density $\epsilon_{\text{vac}} = \epsilon_{\text{vac}}^B - \epsilon_{\text{vac}}^{B=0}$ from the ϵ_n terms in h_n via proper regularization; see Appendix B for details. Here we only remark that this ϵ_{vac} provides another way to derive α_m^{vac} : Setting $B \rightarrow B + A_{12}$ in ϵ_{vac} and expanding it to second order in A_{12} yields precisely the regularized expression (2.24) for α_m^{vac} .

We are now ready to write down the electromagnetic response of graphene. Let us suppose that the electrons fill up an integral number ν of Landau levels, with uniform density $\langle \rho \rangle \equiv \bar{\rho} = \nu/(2\pi\ell^2)$; the case of holes is treated analogously. We take both spin and pseudospin into account, and write $\nu = \sum_n \nu_n$ in terms of the filling factors ν_n of the n th level [$0 \leq \nu_n \leq 4$ for $n \geq 1$ and $0 \leq \nu_{0+} \leq 2$]. The long-wavelength response of graphene is then summarized by the Lagrangian

$$L_A = \bar{\rho} e A_0 - e^2 \ell^2 \bar{\rho} \frac{1}{2} \epsilon^{\mu\nu\rho} A_\mu \partial_\nu A_\rho + \frac{1}{2} \alpha_e(\nu) \mathbf{E}^2 - \frac{1}{2} \alpha_m(\nu) (A_{12})^2 \quad (2.27)$$

with the susceptibilities

$$\alpha_e(\nu) = \frac{3e^2}{2\pi\omega_c} \left[\sum_{n=1}^{\infty} \nu_n \sqrt{n} + 4G(0) \right], \quad (2.28)$$

$$\alpha_m(\nu) = (v_F^2/2) \alpha_e(\nu). \quad (2.29)$$

For clarity we shall from now on display formulas with $m \rightarrow 0$. The vacuum susceptibility α_e^{vac} is almost comparable to the contribution of a single filled $n = 1$ level, i.e., 4×0.21 vs 1. Curiously, in contrast, the $n = 0_{\pm}$ levels hardly contribute to $\alpha_e(\nu)$; their tiny fraction $\propto (\nu_{0+} - 2)(\sqrt{2}/3)|m|\ell$ in α_e shows that a mass gap works to reduce α_e , as is clear intuitively.

III. LONG-WAVELENGTH EFFECTIVE THEORY

In this section we derive an effective gauge theory of graphene in a magnetic field. It is constructed, via functional bosonization²³, so as to reproduce the response (2.27). Such an effective theory has some advantages^{23,24}: It allows one to handle the Coulomb interaction exactly. It readily admits inclusion of vortices, and is thus applicable to the description of the fractional QH effect as well. It furthermore unifies²⁵ the composite-boson²⁶ and composite-fermion²⁷ descriptions of the fractional QH effect.

Applying²⁵ the standard procedure of functional bosonization to the response (2.27) yields an effective theory of a vector field $b_\mu = (b_0, b_1, b_2)$, with the Lagrangian to $O(\partial^2)$,

$$L_b = \frac{1}{2\ell^2\bar{\rho}} b_\mu \epsilon^{\mu\nu\lambda} \partial_\nu b_\lambda + \frac{1}{\ell^2} b_0 + \frac{1}{2\ell^2\bar{\rho}\omega_{\text{eff}}} \left\{ (b_{k0})^2 - \frac{1}{2} v_F^2 (b_{12})^2 \right\} \quad (3.1)$$

and the *effective* cyclotron frequency

$$\omega_{\text{eff}} = e^2 \ell^2 \bar{\rho} / \alpha_e(\nu) = \omega_c g(\nu), \quad g(\nu) \approx \frac{1}{3} \frac{\nu}{\sum_{n=0}^{\infty} \nu_n \sqrt{n} + 4G(0)}, \quad (3.2)$$

where $b_{\mu\nu} = \partial_\mu b_\nu - \partial_\nu b_\mu$; $\ell^2 \bar{\rho} = \nu/(2\pi)$ and $\nu = \sum_{n=0}^{\infty} \nu_n$. The Coulomb interaction and coupling to A_μ are incorporated into this theory, with the Lagrangian

$$L_{\text{eff}}[b] = -e A_\mu \epsilon^{\mu\nu\lambda} \partial_\nu b_\lambda - \frac{1}{2} \delta b_{12} v \delta b_{12} + L_b, \quad (3.3)$$

where $\delta b_{12} v \delta b_{12} = \int d^2 \mathbf{x}' \delta b_{12}(x) v(\mathbf{x} - \mathbf{x}') \delta b_{12}(x')$ for short and $\delta b_{12} = b_{12} - \bar{\rho}$.

This effective theory reproduces the original response (2.27), and actually more: The $A\epsilon\partial A$, \mathbf{E}^2 and $(A_{12})^2$ terms acquire a common kernel so that, e.g., $\mathbf{E}^2 \rightarrow \mathbf{E} \mathcal{K} \mathbf{E}$, with

$$\mathcal{K} = \omega_{\text{eff}}^2 / [\omega_{\text{eff}}^2 + \partial_t^2 - (\omega_{\text{eff}} \ell^2 \bar{\rho} v_{\mathbf{p}} + \alpha_m / \alpha_e) \nabla^2]. \quad (3.4)$$

This shows that the Coulomb interaction $v_{\mathbf{p}} \sim e^2/|\mathbf{p}|$ substantially modifies the dispersion of the cyclotron mode at long wavelengths $\mathbf{p} \rightarrow 0$,

$$\omega(\mathbf{p}) \approx \omega_{\text{eff}} + \frac{1}{2} (\ell^2 \bar{\rho} v_{\mathbf{p}} + \frac{v_F^2}{2\omega_{\text{eff}}}) \mathbf{p}^2. \quad (3.5)$$

For graphene the Landau levels are not equally spaced and the excitation gaps depend on the level index n or ν . When the n th levels are occupied, i.e., at $\nu = 4n + 2$, the minimum activation gap is $\Delta\omega_c^{(n)} = \epsilon_{n+1} - \epsilon_n = (\sqrt{n+1} - \sqrt{n})\omega_c$; numerically, $\Delta\omega_c^{(0)} = 1.0\omega_c$, $\Delta\omega_c^{(1)} \approx 0.4142\omega_c$, $\Delta\omega_c^{(2)} \approx 0.3178\omega_c$, $\Delta\omega_c^{(3)} \approx 0.2679\omega_c$, for $\nu = 2, 6, 10, 14$, respectively. The ω_{eff} in Eq. (3.2) represents such an excitation gap.

For $\nu = 2$, $g(2) = 1/\{6G(0)\} \approx 0.802$, which comes solely from the vacuum fluctuations, appreciably deviates from the number 1.0 quoted above. For $\nu = 6$, $g(6) \approx 0.4141$; for $\nu = 10, 14, \dots$, $g(\nu)$ almost precisely agrees with the quoted numbers, and the agreement becomes exact for $\nu \rightarrow \infty$. It is somewhat surprising that an effective theory constructed from the long-wavelength response alone gives an excellent description of the excitation spectrum.

In other words, the effective theory reveals a general link: The susceptibility α_e of a QH system is essentially determined by a Hall conductance and the Landau gap,

$$\alpha_e(\nu) = (e^2/2\pi) \nu / \omega_{\text{eff}} = \sigma_{\text{Hall}} / \Delta\omega_c^{(n)}. \quad (3.6)$$

This implies that $\alpha_e(\nu)$ rises linearly with ν for typical QH systems with equally-spaced Landau levels while it grows more rapidly for graphene,

$$\alpha_e(\nu) \propto \nu^{3/2}. \quad (3.7)$$

Actually, formula (3.6) is a condensed-matter realization of the related fact²⁸ in relativistic field theory that in 2+1 dimensions the gauge field acquires a mass from the CS term in the presence of the Maxwell term $\sim \mathbf{E}^2$.

IV. POLARIZATION FUNCTION

We have seen that the vacuum component α_e^{vac} constitutes an appreciable portion of the susceptibility $\alpha_e(\nu)$.

In this section we examine the effect of polarization at shorter wavelengths and extract some observable consequences. We shall see that the screening properties of graphene in a magnetic field are substantially different from those of graphene without the magnetic field, discussed recently²⁹.

Let us turn off the Coulomb interaction for the moment and calculate the polarization function $P(\mathbf{p}, \omega) \equiv -i \langle \rho(x) \rho(y) \rangle^{\text{F.T.}}$, where F.T. stands for the Fourier transform. To this end we denote by $P_n(\mathbf{p}, \omega) = -i \langle n | T \rho(x) \rho(y) | n \rangle^{\text{F.T.}}$ the polarization function for the filled n th Landau level $|n\rangle = \{|n, y_0\rangle\}$ and write it as a regularized sum $P_n(\mathbf{p}, \omega) = \sum_{k=-N}^N P_n^k(\mathbf{p}, \omega)$ over components P_n^k coming from the virtual ($n \rightarrow k \rightarrow n$) transitions. As before, we truncate the spectrum to a finite interval $-N \leq n, k \leq N$. From Eq. (2.10) one finds

$$P_n^k(\mathbf{p}, \omega) = -\left\{ \frac{1}{\epsilon_{kn} - \omega} + \frac{1}{\epsilon_{kn} + \omega} \right\} \sigma_n^k(\mathbf{p}), \quad (4.1)$$

$$\sigma_n^k(\mathbf{p}) = \frac{1}{2\pi\ell^2} e^{-\frac{1}{2}\ell^2\mathbf{p}^2} g_{nk}(\mathbf{p}) g_{kn}(-\mathbf{p}), \quad (4.2)$$

where $\epsilon_{kn} = \epsilon_k - \epsilon_n$; $\sigma_n^k(\mathbf{p})$ is the spectral weight.

One can calculate the response $P(\mathbf{p}, \omega) = \sum_n P_n(\mathbf{p}, \omega)$ by selectively summing P_n^k over occupied levels $\{n\}$ and unoccupied levels $\{k\}$ for a given graphene state. In practice, it is advantageous, especially for numerical evaluations, to calculate $P_n = \sum_{k=-N}^N P_n^k$ by summing over all levels $\{k\}$ since Fermi statistics is automatically taken care of in the regularized sum, as noted in the previous section. We focus on the real part of $P_n(\mathbf{p}, \omega)$ in the static limit $\omega \rightarrow 0$ below. For the ψ sector the result is

$$P_n(\mathbf{p}, 0) = -\frac{3\mathbf{p}^2}{2\pi\omega_c} s_n \hat{\xi}_n(\mathbf{p}^2), \quad (4.3)$$

$$\hat{\xi}_n(\mathbf{p}^2) = e^{-\frac{1}{2}\ell^2\mathbf{p}^2} \sqrt{|n|} \xi(\frac{1}{2}\ell^2\mathbf{p}^2, |n|), \quad (4.4)$$

with

$$\begin{aligned} & 6\xi(x, n) \\ &= \sum_{k=1}^{N-n} \frac{(n-1)!}{(n+k-1)!} \frac{x^{k-1}}{k} \left[(L_n^{(k)} + L_{n-1}^{(k)})^2 - \frac{k}{n+k} (L_n^{(k)})^2 \right] \\ & - \sum_{k=1}^{n-1} \frac{(n-k)!}{n!} \frac{x^{k-1}}{k} \left[(L_{n-k}^{(k)} + L_{n-k-1}^{(k)})^2 \right. \\ & \quad \left. + \frac{k}{n-k} (L_{n-k-1}^{(k)})^2 \right] \\ & - \frac{x^{n-1}}{n!n} - \frac{1}{4nx} (L_n - L_{n-1})^2 \quad (\text{for } n \geq 1), \end{aligned} \quad (4.5)$$

and $\xi(x, n=0) = 0$, where $L_n^{(k)} = L_n^{(k)}(x)$ for short; $\xi(x, n)$ are normalized so that $\xi(0, n) = 1$ for $1 \leq n \leq N-1$, with their reference to the cutoff N suppressed. Note that $P_{-n} = -P_n$; in particular, $P_0 = 0$, i.e., the $n = 0_{\pm}$ levels do not contribute to polarization (for $m \rightarrow 0$).

One can now write $P(\mathbf{p}, 0)$ or the static susceptibility function $\alpha_e[\mathbf{p}] = -(e^2/\mathbf{p}^2) P(\mathbf{p}, 0)$ for graphene as

$$\alpha_e[\mathbf{p}] = \frac{3e^2}{2\pi\omega_c} \left[\sum_{n>0} \nu_n \hat{\xi}_n(\mathbf{p}^2) + 4\hat{\xi}^{\text{vac}}(\mathbf{p}^2) \right], \quad (4.6)$$

where $\hat{\xi}^{\text{vac}}(\mathbf{p}^2) = -\sum_{n=1}^N \hat{\xi}_n(\mathbf{p}^2)$. This $\alpha_e[\mathbf{p}]$ is correctly reduced to α_e in Eq. (2.28) for $\mathbf{p} \rightarrow 0$.

Let us now turn on the Coulomb interaction $v_{\mathbf{p}} = 2\pi\alpha/(\epsilon_b|\mathbf{p}|)$ and study its effects in the RPA. The RPA dielectric function is written as

$$\epsilon(\mathbf{p}, \omega) = 1 - v_{\mathbf{p}} P(\mathbf{p}, \omega), \quad (4.7)$$

and the RPA polarization function $P_{\text{RPA}}(\mathbf{p}, \omega) = P(\mathbf{p}, \omega)/\epsilon(\mathbf{p}, \omega)$ is screened through $\epsilon(\mathbf{p}, \omega)$. The static dielectric function then reads

$$\epsilon(\mathbf{p}, 0) = 1 + \frac{3\alpha}{\epsilon_b v_F} \frac{\ell|\mathbf{p}|}{\sqrt{2}} \left[\sum_{n>0} \nu_n \hat{\xi}_n(\mathbf{p}^2) + 4\hat{\xi}^{\text{vac}}(\mathbf{p}^2) \right], \quad (4.8)$$

where $\alpha = e^2/(4\pi\epsilon_0) \approx 1/137$ and $v_F \approx c/300$. With air on one side of the graphene plane and SiO_2 on the other, the unscreened dielectric constant is estimated⁸ to be $\epsilon_b \approx 2/(\epsilon_{\text{air}}^{-1} + \epsilon_{\text{SiO}_2}^{-1}) \approx 1.6$ with $\epsilon_{\text{air}} \approx 1$ and $\epsilon_{\text{SiO}_2} \approx 4$; this yields an estimate of the coefficient

$$3\alpha/(\epsilon_b v_F) = 3\sqrt{2}\alpha/(\epsilon_b \ell\omega_c) \approx 4.1. \quad (4.9)$$

In Fig. 1 we plot $\alpha_e[\mathbf{p}]$ and $\epsilon(\mathbf{p}, 0) - 1$ for $\nu = 0, 2, 6, 10, 14$. Note first that there is no screening at long distances, $\epsilon(\mathbf{p}, 0) \rightarrow 1$ for $\mathbf{p} \rightarrow 0$, as is typical of two-dimensional systems. However, $\epsilon(\mathbf{p}, 0)$ grows rapidly with $|\mathbf{p}|$ and becomes sizable for $|\mathbf{p}|\ell \sim 1$, with its peak value $\epsilon(\mathbf{p}, 0) \approx 3.4 \sim 20$ for $\nu = 0 \sim 14$. For comparison, analogous plots for a standard (GaAs) QH system³⁰ (per spin) are shown in Fig. 2. Both $\alpha_e[\mathbf{p}]$ and $\epsilon(\mathbf{p}, 0) - 1$ look qualitatively similar in the two cases, but there are clear differences: First, for graphene even the vacuum (with $\nu = 0$) has a finite polarization, which decreases only gradually with increasing $|\mathbf{p}|\ell$; this reflects the fact that the Dirac sea has quantum fluctuations of a whole range of wavelengths. Second, for graphene $\alpha_e[\mathbf{p}]$ and $\epsilon(\mathbf{p}, 0)$ grow fast with ν . This reflects the Landau-level characteristic of graphene; the quantum effect grows as the level gaps become narrower.

To compare graphene and GaAs systems let us note the following: For GaAs $\omega_c = eB/m^* \approx 20 B[\text{T}] \text{ K}$ is considerably smaller than for graphene while the substrate dielectric constant $\epsilon_b \approx 12.9 \gg (\epsilon_b)_{\text{graphene}} \approx 1.6$ so that

$$(\epsilon_b \omega_c)_{\text{GaAs}}/(\epsilon_b \omega_c)_{\text{graphene}} \approx 0.4 \sqrt{B[\text{T}]}. \quad (4.10)$$

Figure 2 indicates that the effect of polarization is generally not quite appreciable for the GaAs system, with $\epsilon(\mathbf{p}, 0) \approx 1.7 \sim 2.2$ at $|\mathbf{p}|\ell \sim 1$ for $\nu = 1 \sim 3$ if we take $3\sqrt{2}\alpha/(\epsilon_b \ell\omega_c) \approx 4$, which, in view of Eqs. (4.9) and (4.10), would overestimate $\epsilon(\mathbf{p}, 0)$ numerically over a typical range of the applied magnetic field $B > 10 \text{ T}$.

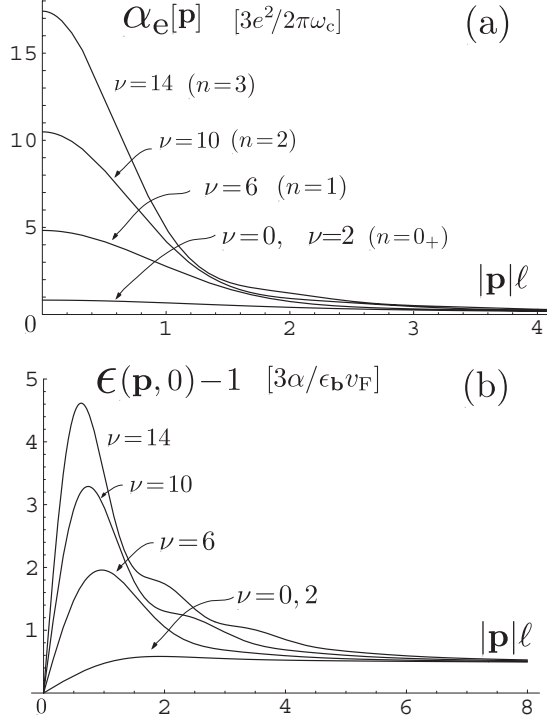


FIG. 1: (a) Susceptibility $\alpha_e[\mathbf{p}]$ for graphene at integer fillings ν , plotted in units of $3e^2/(2\pi\omega_c)$; n refers to the highest occupied Landau level. (b) Dielectric function $\epsilon(\mathbf{p}, 0) - 1$ is plotted in units of $3\alpha/(\epsilon_b v_F) \approx 4.1$ so that the peak value of $\epsilon(\mathbf{p}, 0)$ ranges from 3.4 to 20 for $\nu = 0 \sim 14$.

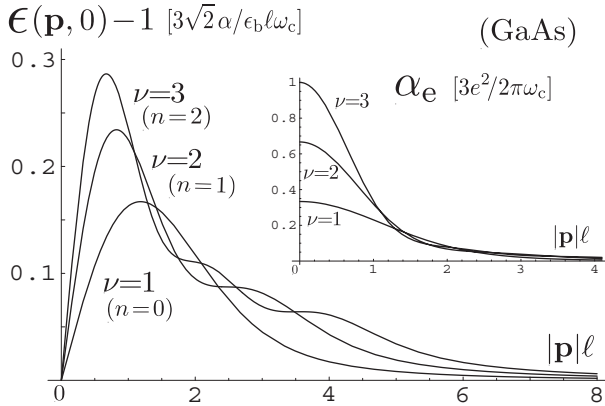


FIG. 2: Susceptibility $\alpha_e[\mathbf{p}]$ and $\epsilon(\mathbf{p}, 0) - 1$ for a GaAs system (per spin). The peak value of $\epsilon(\mathbf{p}, 0)$ ranges from 1.7 \sim 2.2 for $\nu = 1 \sim 3$ if one takes $3\sqrt{2}\alpha/(\epsilon_b \ell \omega_c) \approx 4$.

One can derive³⁰ the excitation spectrum corrected by the Coulomb interaction from the RPA response $P_{\text{RPA}}(\mathbf{p}, \omega) = P(\mathbf{p}, \omega)/\epsilon(\mathbf{p}, \omega)$. Let us isolate from $P(\mathbf{p}, \omega)$ one of its poles at $\omega \sim \epsilon_{kn} = \epsilon_k - \epsilon_n$ and set $\epsilon(\mathbf{p}, \omega) = 1 - v_{\mathbf{p}} P(\mathbf{p}, \omega) \rightarrow 0$. This fixes the pole position of the RPA response function, $\epsilon_{k,n}^{\text{RPA}} = \epsilon_k - \epsilon_n + \Delta\epsilon_{k,n}(\mathbf{p})$ with

$$\Delta\epsilon_{k,n}(\mathbf{p}) \approx \frac{\alpha}{\epsilon_b \ell} \nu_g(\mathbf{p}) \ell |\mathbf{p}| / \{2 \epsilon(\mathbf{p}, 0)\}, \quad (4.11)$$

$$\nu_g(\mathbf{p}) = \sum g_{nk}(-\mathbf{p}) g_{kn}(\mathbf{p}) e^{-x}/x, \quad (4.12)$$

where $x = \frac{1}{2} \ell^2 \mathbf{p}^2$; the sum is taken over possible (k, n) that lead to the gap $\epsilon_k - \epsilon_n$. We have parametrized $\Delta\epsilon_{k,n}(\mathbf{p})$ so that $\nu_g(0)$ corresponds to $\nu = 2\pi \ell^2 \bar{\rho}$ in the excitation spectrum (3.5) of the effective theory. Note that $\Delta\epsilon_{k,n}(\mathbf{p} \rightarrow 0) = 0$ so that the excitation gap $\epsilon_k - \epsilon_n$ remains unshifted for $\mathbf{p} \rightarrow 0$. The excitation gap $\Delta\omega_c^{(0)} = \omega_c$, in particular, is realized via the $0_{\pm} \rightarrow 1$ or $-1 \rightarrow 0_+$ transitions, yielding

$$\nu_g(\mathbf{p}) = 2 e^{-\frac{1}{2} \ell^2 \mathbf{p}^2} \text{ for } \nu = 0, 2. \quad (4.13)$$

The next gap $\Delta\omega_c^{(1)} \approx 0.14\omega_c$ at $\nu = 6$ is due the $1 \rightarrow 2$ transition, giving $\nu_g(\mathbf{p}) = (1 + \sqrt{2} - x/\sqrt{2})^2 e^{-x}$ with $x = \frac{1}{2} \ell^2 \mathbf{p}^2$. Also the gaps $\Delta\omega_c^{(n)} = (\sqrt{n+1} - \sqrt{n})\omega_c$ open up at $\nu = 4n+2$ via the $n \rightarrow n+1$ transitions with $\nu_g(0) = (\sqrt{n} + \sqrt{n+1})^2$. Actually, these numbers $\nu_g(0)$ and $\nu = 4n+2$ agree within 3 percent for $n = 1$ and the agreement improves rapidly for larger n . This shows that the excitation spectrum (3.5) in the effective theory is practically in good agreement with the RPA result.

In Fig. 3 (a) and (b) we plot the exciton spectra $\Delta\epsilon_{k,n}(\mathbf{p})$ near the energy gaps ω_c , $0.41\omega_c$ and $0.32\omega_c$. The unscreened spectra (dashed curves) are generally peaked around $|\mathbf{p}|\ell \sim 1$ and are efficiently reduced to the screened spectra (solid curves) through $\epsilon(\mathbf{p}, 0)$ also peaked at $|\mathbf{p}|\ell \sim 1$. Near the gap ω_c at $\nu = 0, 2$ the spectrum is about one third of the unscreened one in magnitude. The effect of screening is far more prominent at higher ν . Near the gap $0.41\omega_c$ at $\nu = 6$ the spectrum is about one order of magnitude smaller than the unscreened one. Near the gap $0.32\omega_c$ at $\nu = 10$ the spectrum is even lower than the $\nu = 6$ spectrum although the unscreened spectra are opposite in magnitude.

For comparison Fig. 3 (c) shows the exciton spectra in the GaAs QH system³⁰ near the energy gap $\omega_c = eB/m^*$ at $\nu = 1, 2$. There the spectra are reduced roughly by 50 percent or less. Clearly the effect of screening is not quite important for GaAs systems.

V. SUMMARY AND DISCUSSION

In this paper we have examined the electromagnetic characteristics of graphene in a magnetic field to explore possible signatures of quantum field theory in the low-energy dynamics of graphene. The key features that

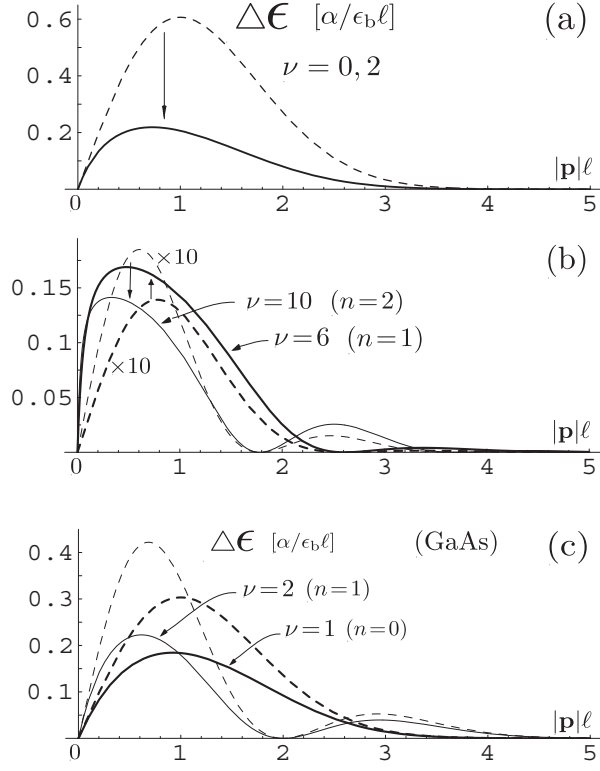


FIG. 3: (a) Excitation spectrum near the gap ω_c at $\nu = 0$ and 2, plotted in units of $\alpha/\epsilon_b\ell$. It is reduced from the bare spectrum (dashed curve) via screening. (b) Excitation spectra near the gap $0.41\omega_c$ and $0.32\omega_c$ at $\nu = 6$ and $\nu = 10$, respectively. The unscreened spectra (dashed curves) are one order of magnitude larger than those depicted in the figure. (c) Excitation spectra for a GaAs system per spin, with the choice $3\sqrt{2}\alpha/(\epsilon_b\ell\omega_c) \approx 4$.

distinguish graphene from standard QH systems are (1) the quantum nature of the graphene ground state (vacuum) and (2) the relativistic pattern of Landau levels ($\alpha \pm \sqrt{|n|}$) with gaps decreasing with the level index n .

The graphene vacuum is a dielectric medium with electron and hole pairs created (from the depth of the Dirac sea) in response to an applied field. In particular, the electric and magnetic susceptibilities (α_e, α_m) and the dielectric function $\epsilon(\mathbf{p}, \omega) - 1$ are nonzero for the vacuum over a whole range of wavelengths and grow prominently with increasing filling factor ν in a way that reflects the Landau-level characteristics (2) of graphene.

As for experimental verification, detection of the inter-Landau-level cyclotron-mode excitations, or excitons, from the $\nu = 0$ ground state through light absorption or reflection would be a direct signal for the quantum nature of the vacuum. A detailed study of the exciton spectra from the states with $\nu = 0, 2, 6, \dots$ would also reveal the effect of screening around $|\mathbf{p}|\ell \sim 1$, which is expected to be sizable for graphene, as discussed in Sec. IV.

In Sec. II special emphasis has been placed on the need for regularization in calculating quantum corrections for

graphene. We have pointed out that the regularized (linear) response is written as an asymmetry in the spectra of the occupied and unoccupied states, weighted with the response per state; see Eq. (2.16). For the induced CS coupling this spectral asymmetry is related to the η -invariant of the Dirac Hamiltonian (i.e., the difference in number between positive and negative eigenvalues¹²), although it vanishes for graphene eventually. For the susceptibilities or the polarization function, in contrast, there is no such underlying index theorem but the spectral asymmetry yields nonzero results for them, with the contribution from each level adding up. In this connection, some peculiarities of the $n = 0_{\pm}$ Landau levels would be worth noting. While they carry the (normal) Hall conductance $\pm e^2/h$ per level, they hardly contribute to susceptibilities α_e and α_m (for $m \rightarrow 0$). As a result, it is essentially the vacuum state that would govern the dielectric property of graphene for $|\nu| \leq 2$; the effect of polarization would be insensitive to carrier densities over this range; see, e.g., Eq. (4.13).

In Sec. III we have seen that an effective gauge theory of graphene, constructed from the long-wavelength response, gives an excellent description of the excitation spectrum. In this effective theory graphene and other QH systems look quite similar, except that the effective Landau gap $\Delta\omega_c \sim \omega_{\text{eff}}$ in Eq. (3.2) now depends on ν for graphene. We have thereby noted a general relation $\alpha_e \approx \sigma_{\text{Hall}}/\omega_{\text{eff}}$ which relates the susceptibility α_e to the Hall conductance and the Landau gap.

Acknowledgments

The author wishes to thank A Sawada for useful discussion. This work was supported in part by a Grant-in-Aid for Scientific Research from the Ministry of Education Science and Culture of Japan (Grant No. 17540253).

APPENDIX A: FREE DIRAC ELECTRONS

In this appendix we summarize the eigenmodes of the Dirac Hamiltonian in a magnetic field. Let us focus on the ψ field governed by $\mathcal{H}_+ = v_F(\sigma_1\Pi_1 + \sigma_2\Pi_2 + m\sigma_3)$ in Eq. (2.1) with $A_i \rightarrow \mathbf{A}^B = B(-y, 0)$. The spectrum of ψ consists of an infinite tower of Landau levels of energy $\epsilon_n = s_n \omega_c \sqrt{|n| + m^2\ell^2/2}$ labeled by integers $n = 0, \pm 1, \pm 2, \dots$, with $\ell = 1/\sqrt{eB}$ and $s_n \equiv \text{sign}\{n\} = \pm 1$. The positive-energy ($n > 0$) and negative-energy ($n < 0$) eigenmodes are neatly cast in the unified form

$$\psi_{ny_0}(\mathbf{x}) = \frac{1}{\sqrt{2}} \begin{pmatrix} c_n^+ \phi_{|n|-1}(y-y_0) \\ s_n c_n^- \phi_{|n|}(y-y_0) \end{pmatrix} \frac{1}{\sqrt{2\pi\ell^2}} e^{ixy_0/\ell^2}, \quad (\text{A1})$$

where $y_0 \equiv \ell^2 p_x$ and $c_n^{\pm} = \sqrt{1 \pm v_F m/\epsilon_n}$, in terms of the standard wave functions $\propto \phi_n(y-y_0) e^{ixp_x}$ of the

nonrelativistic case. For $m > 0$ the $n = 0$ eigenmodes

$$\psi_{0-,y_0}(\mathbf{x}) = \begin{pmatrix} 0 \\ -\phi_0(y-y_0) \end{pmatrix} \frac{1}{\sqrt{2\pi\ell^2}} e^{ixy_0/\ell^2} \quad (\text{A2})$$

describe negative-energy electrons with $\epsilon_{0-} = -v_F m$. For the parity partner χ , the spectrum and eigenmodes are obtained by reversing the sign of m . The $n = 0$ modes are actually the $n = 0_+$ modes $\chi_{0+,y_0}(\mathbf{x}) \sim (0, \phi_0)^t$ which describe electrons with positive energy $\epsilon_{0+} = v_F m$.

APPENDIX B: VACUUM ENERGY

In this appendix we outline the calculation of the vacuum energy in a magnetic field B , discussed somewhere below Eq. (2.26). Via normal ordering in H , one obtains the vacuum energy per unit area

$$\epsilon_{\text{vac}}^B = \frac{1}{2\pi\ell^2} \left(-\frac{1}{2}\right) \left(2 \sum_{n=1}^N \epsilon_n + |m|v_F\right). \quad (\text{B1})$$

This is to be compared with the energy density in the ordinary ($B = 0$) vacuum, $\epsilon_{\text{vac}}^{B=0} = (-\frac{1}{2})2v_F \sum_{\mathbf{k}} \sqrt{\mathbf{k}^2 + m^2}$ with the Fermi momentum k_F chosen to give the same number of states, $N_s = k_F^2/(2\pi) = (2N+1)/(2\pi\ell^2)$, as in the $B \neq 0$ case. The observable vacuum energy density $\epsilon_{\text{vac}} = \epsilon_{\text{vac}}^B - \epsilon_{\text{vac}}^{B=0}$ thereby becomes finite for $N \rightarrow \infty$,

$$\begin{aligned} \epsilon_{\text{vac}} &= \frac{\omega_c}{2\pi\ell^2} \left[-\sum_{n=1}^N \sqrt{n+\lambda} - \frac{1}{2}\sqrt{\lambda} \right. \\ &\quad \left. - \frac{2}{3}\lambda^{3/2} + \frac{2}{3}(N + \frac{1}{2} + \lambda)^{3/2} \right], \\ &= \frac{\omega_c}{2\pi\ell^2} \left[-\zeta(-\frac{1}{2}) - \frac{1}{2}\sqrt{\lambda} + \dots \right], \end{aligned} \quad (\text{B2})$$

where $\lambda = \frac{1}{2}m^2\ell^2$ and $-\zeta(-\frac{1}{2}) \approx 0.2079$. The χ sector also leads to the same ϵ_{vac} .

-
- ¹ K. S. Novoselov, A. K. Geim, S. V. Morozov, D. Jiang, M. I. Katsnelson, I. V. Grigorieva, S. V. Dubonos, and A. A. Firsov, *Nature* (London) **438**, 197 (2005).
 - ² Y. Zhang, Y.-W. Tan, H. L. Stormer, and P. Kim, *Nature* (London) **438**, 201 (2005).
 - ³ Y. Zhang, Z. Jiang, J.P. Small, M.S. Purewal, Y.-W. Tan, M. Fazlollahi, J.D. Chudow, J.A. Jaszczak, H. L. Stormer, and P. Kim, *Phys. Rev. Lett.* **96**, 136806 (2006).
 - ⁴ Y. Zheng and T. Ando, *Phys. Rev. B* **65**, 245420 (2002).
 - ⁵ V. P. Gusynin and S. G. Sharapov, *Phys. Rev. Lett.* **95**, 146801 (2005).
 - ⁶ N. M. R. Peres, F. Guinea, and A. H. CastroNeto, *Phys. Rev. B* **73**, 125411 (2006).
 - ⁷ K. Nomura and A. H. MacDonald, *Phys. Rev. Lett.* **96**, 256602 (2006).
 - ⁸ J. Alicea and M. P. A. Fisher, *Phys. Rev. B* **74**, 075422 (2006).
 - ⁹ V. P. Gusynin, V. A. Miransky, S. G. Sharapov, and I. A. Shovkovy, *Phys. Rev. B* **74**, 195429 (2006); see also, E. V. Gorbar, V. P. Gusynin, V. A. Miransky, and I. A. Shovkovy, *Phys. Rev. B* **66**, 045108 (2002).
 - ¹⁰ J.-N. Fuchs and P. Lederer, *Phys. Rev. Lett.* **98**, 016803 (2007).
 - ¹¹ A. N. Redlich, *Phys. Rev. Lett.* **52**, 18 (1984); R. Jackiw, *Phys. Rev. D* **29**, 2375 (1984).
 - ¹² A. J. Niemi and G. W. Semenoff, *Phys. Rev. Lett.* **51**, 2077 (1983).
 - ¹³ G. W. Semenoff, *Phys. Rev. Lett.* **53**, 2449 (1984).
 - ¹⁴ S. M. Girvin and T. Jach, *Phys. Rev. B* **29**, 5617 (1984).
 - ¹⁵ K. Shizuya, *Phys. Rev. B* **45**, 11 143 (1992).
 - ¹⁶ S. M. Girvin, A. H. MacDonald, P. M. Platzman, *Phys. Rev. B* **33**, 2481 (1986).
 - ¹⁷ M. V. Berry, *Proc. R. Soc. London, Ser. A* **392**, 45 (1984).
 - ¹⁸ As in the Tomonaga-Luttinger model, the infinite depth of the Dirac sea is an artifact of the continuum model (2.1) whose validity is limited to a (far) smaller energy range than the original lattice model. It is this energy range that sets the scale of the spectrum cutoff, and regularization provides a controlled way to derive the (low-energy) response independent of the cutoff.
 - ¹⁹ N. Fumita and K. Shizuya, *Phys. Rev. D* **49**, 4277 (1994).
 - ²⁰ To be precise, it is the real part of the response (such as $V_n^{(2)}$ that enjoys this property; obviously, it is not shared by the imaginary part.
 - ²¹ F. D. M. Haldane, *Phys. Rev. Lett.* **61**, 2015 (1988).
 - ²² To be precise, η_{-N} becomes insensitive to the transitions across the Dirac sea when the four possible types of transitions ($-N \rightarrow N \pm 1$) and ($-N \rightarrow N \pm 2$) are combined.
 - ²³ E. Fradkin and F. A. Schaposnik, *Phys. Lett. B* **338**, 253 (1995); F. A. Schaposnik, *Phys. Lett. B* **356**, 39 (1995).
 - ²⁴ D.-H. Lee and S.-C. Zhang, *Phys. Rev. Lett.* **66**, 1220 (1991).
 - ²⁵ K. Shizuya, *Phys. Rev. B* **63**, 245301 (2001); *ibid.* **65**, 205324 (2002); *Int. J. Mod. Phys. B* **17**, 5875 (2003).
 - ²⁶ S. C. Zhang, *Int. J. Mod. Phys. B* **6**, 25 (1992).
 - ²⁷ J. K. Jain, *Phys. Rev. Lett.* **63**, 199 (1989); A. Lopez and E. Fradkin, *Phys. Rev. B* **44**, 5246 (1991); B. I. Halperin, P. A. Lee and N. Read, *Phys. Rev. B* **47**, 7312 (1993).
 - ²⁸ S. Deser, R. Jackiw, and S. Templeton, *Ann. Phys. (N.Y.)* **140**, 372 (1982).
 - ²⁹ T. Ando, *J. Phys. Soc. Jpn.* **75**, 074716 (2006); E. H. Hwang and S. Das Sarma, *cond-mat/0610561*; B. Wunsch, T. Stauber, F. Sols, and F. Guinea, *New. J. Phys.* **8**, 318 (2006).
 - ³⁰ C. Kallin and B. I. Halperin, *Phys. Rev. B* **30**, 5655 (1984).